Supporting Information

Naik et al. 10.1073/pnas.1319446111

SI Text

1. Optimization of Cubic (Al,Sc)N Sandwiched Between Titanium Nitride Layers

Titanium nitride (TiN)–(Al,Sc)N superlattices were deposited using reactive dc magnetron sputtering on (001) MgO substrates. Superlattices with different compositions of (Al,Sc)N were grown to optimize the properties of the (Al,Sc)N. The superlattices were characterized using spectroscopic ellipsometry, X-ray diffraction, and transmission electron microscopic (TEM) imaging. Optimum composition was expected to be around 30% Sc, which can match the lattice of TiN. Performing optimization on the properties of (Al,Sc)N showed that $Al_{0.72}Sc_{0.28}N$ has desirable properties as a dielectric material for hyperbolic metamaterials (HMMs). Sc concentration higher than 28 at % caused red-shift in the absorption band-edge increasing optical losses in (Al,Sc)N layers at the wavelength of interest (720 nm). Reducing Sc concentration makes it increasingly more difficult to stabilize (Al,Sc)N in a rocksalt lattice. It was found that $Al_{0.72}Sc_{0.28}N$ can be stabilized in a rocksalt lattice for thicknesses up to a micrometer, and also exhibit reasonably low optical losses at 720 nm wavelength. TiN and (Al,Sc)N of optimum composition were deposited to form superlattice consisting of 20-nm-thick TiN layers and varying thickness (Al,Sc)N layers. The cross-section TEM image of the superlattice with varying thickness of $Al_{0.72}Sc_{0.28}N$ layers is shown in Fig. S1. It may be noticed that smooth and crystalline layers of (Al,Sc)N may be formed with thickness as small as 2 nm. Also, the interfaces are sharp as can be noticed from the figure.

2. Reflectance and Transmittance Measurements and Calculations

Reflectance and transmittance from superlattice samples were also measured using the ellipsometer (V-VASE, J.A. Woollam Co.). Both of these measurements were made in the wavelength range 300–1000 nm. The angle of incidence was varied in the range 20–76° for reflectance and 0–76° for transmittance. The measured reflectance and transmittance can serve as checkpoints assuring the reliability of the material parameters retrieved from ellipsometry (Fig. 1 *A* and *B*). Using the optical properties of TiN and (Al,Sc)N retrieved from ellipsometry, transfer-matrix-based calculations were used to numerically evaluate the angular reflectance and transmittance of the superlattice. Fig. S2 *A* and *B* shows the measured reflectance and transmittance, whereas Fig. S2 *C* and *D* shows the calculated reflectance and transmittance. The measured quantities agree reasonably well with the calculated quantities. This assures that the optical properties of TiN and (Al,Sc)N shown in Fig. 1 *A* and *B* are reasonably accurate. The effective medium properties shown in Fig. 1 *C* and *D*, which rely upon the dielectric functions of TiN and (Al,Sc)N through Eq. **S1**, are also reliable.

$$\begin{aligned} \varepsilon_{\|} &= f_m \varepsilon_m + (1-f_m)\varepsilon_d \\ (\varepsilon_{\perp})^{-1} &= f_m(\varepsilon_m)^{-1} + (1-f_m)(\varepsilon_d)^{-1}, \end{aligned} \quad \textbf{[S1]}$$

where ε_m and ε_d are permittivities of metal and dielectric, respectively, and f_m is the volume fill-fraction of metal.

3. Optical Properties of Epitaxial and Polycrystalline Films

TiN films on (100) silicon grow polycrystalline unless a buffer layer of thick (>50 nm) TiN layer or MgO is used (1, 2). To study the properties of the polycrystalline superlattices, TiN–(Al,Sc)N alternating layers, each 10 nm thick, were deposited on both silicon (100) and MgO (001) substrates. X-ray diffraction and TEM characterization showed that the superlattice on silicon had a polycrystalline structure and rougher interfaces, whereas the one on MgO had an epitaxial structure and sharp interfaces. The optical properties of both of these samples were measured using ellipsometry and the dielectric functions of the constituent materials retrieved from these data are as shown in Fig. S3. A polycrystalline TiN film has a smaller roll-off in its real permittivity and slightly higher imaginary permittivity than the epitaxial film. (Al,Sc)N layers relax into the wurtzite structure in polycrystalline multilayers and hence their optical properties are substantially different. Wurtzite (Al,Sc)N has a smaller real permittivity and red-shifted absorption edge which results in larger optical losses in the visible range. These properties of the constituent materials make the polycrystalline superlattice inferior in its performance as an HMM in the visible range. Nevertheless, it exhibits hyperbolic dispersion in the visible and longer wavelength ranges and qualifies as an HMM, although having higher losses.

4. Local Density of States Calculations

The total enhancement in decay rate of an emitter in an inhomogeneous medium is calculated by Eq. **S2**. In our case, the upper-half space is assumed to be vacuum, and the lower-half space consists of a spacer layer, HMM, and substrate. The emitter radiates into low-*k* modes that propagate in HMM and vacuum, high-*k* modes that propagate in HMM only and eventually decay as heat. P is the total power radiated by the emitter into all possible modes including heat. P_0 is the power radiated by the same emitter isolated in vacuum.

$$\frac{P}{P_0} = 1 + \frac{6\pi\varepsilon_0}{|\boldsymbol{\mu}|^2}\frac{1}{k^3} Im\{\boldsymbol{\mu}^*.\boldsymbol{E}_s(\boldsymbol{r}_0)\}. \quad \textbf{[S2]}$$

The scattered field $\boldsymbol{E}_s(\mathbf{r})$ is calculated using Green's function formalism (Eq. **S3**) leading to the local density of states form. The Green's function is expanded in the angular form to find its contribution at every $\boldsymbol{k}_{||}$. Using this form, the total power emitted by the dipole may be calculated as given in ref. 3. The equations used to calculate the total normalized power and power radiated into upper-half plane are as shown in Eqs. **S4** and **S5**, respectively.

$$\boldsymbol{E}_s(\boldsymbol{r}) = \left(\frac{\omega^2}{c^2\varepsilon_0}\right)\overleftrightarrow{\boldsymbol{G}}_{ref}(r, r_0)\boldsymbol{\mu}, \quad \textbf{[S3]}$$

$$\begin{aligned} \frac{P}{P_0} &= 1 + \frac{3}{4} f_{\|}^2 \int_0^{\infty} Re\left\{\left(\frac{k_{\|}}{k_{\perp}} r^s - k_{\|}k_{\perp} r^p\right) e^{2ik_{\perp}h}\right\} dk_{\|} \\ &+ \frac{3}{2} f_{\perp}^2 \int_0^{\infty} Re\left\{\frac{k_{\|}^3}{k_{\perp}} r^p e^{2ik_{\perp}h}\right\} dk_{\|}, \end{aligned} \quad \textbf{[S4]}$$

$$\begin{aligned} \frac{P_{\uparrow}}{P_0} &= \frac{1}{2} + \frac{3}{8} f_{\|}^2 \int_0^{k_0} \left(k_{\|}k_{\perp}|r^p|^2 + \frac{k_{\|}}{k_{\perp}}|r^s|^2 + 2Re\left\{\left(\frac{k_{\|}}{k_{\perp}} r^s - k_{\|}k_{\perp} r^p\right) e^{2ik_{\perp}h}\right\}\right) dk_{\|} \\ &+ \frac{3}{4} f_{\perp}^2 \int_0^{k_0} \left(\frac{k_{\|}^3}{k_{\perp}}|r^p|^2 + 2Re\left\{\frac{k_{\|}^3}{k_{\perp}} r^p e^{2ik_{\perp}h}\right\}\right) dk_{\|}. \end{aligned} \quad \textbf{[S5]}$$

The power radiated into high-*k* modes is evaluated using Eq. **S4**, with the lower limit of integration set to k_0. Notice that all k values used in Eqs. **S3–S5** are normalized, and $k_0 = 1$ for air or vacuum as the medium of the upper-half plane.

r_s and r_p are Fresnel's reflection coefficients calculated using t-matrix approach for the superlattice system. In our experiments the emitters (dye molecules) are spread in a layer of thickness 11 nm. Hence, in all our calculations, the emitter distance from the surface of the spacer layer is varied from 0 to 11 nm, and the calculated powers are averaged.

5. Lifetime Measurements

Lifetime measurements were performed using a customized confocal microscope with time-correlated single-photon counting technique as described in *Methods*. The lifetime of emitters placed on top of the sample and their fluorescence intensity were spatially mapped on a chosen scan area of the sample. Such measurements were repeated on many different regions of the sample surface and averaged to get the mean lifetime. The samples prepared for the measurement were very homogeneous yielding in a very narrow distribution of the lifetimes measured. A typical map of the lifetime and fluorescence intensity measured on one of the samples is as shown in Fig. S4. The red spots seen in the upper right of the lifetime map are believed to be arising from dust particles settled on the sample during spincoating. The average lifetimes are estimated in the regions excluding such sparsely scattered anomalous spots. The SD in lifetime of the emitters measured on this sample was 0.008 ns. Similarly, on all other samples as well, the SDs of the measured lifetimes were less than 0.012 ns.

6. Radiative Decay Rate and Apparent Quantum Yield Estimations

The radiative decay rate and apparent quantum yield estimations are performed using the method described in ref. 4. Eq. **S6** gives the relationship between the normalized radiative rate (Γ_r) of the emitter and the measured spontaneous emission lifetime (τ), where k_{nr} is the nonradiative decay rate. The absorption (A) measurements were carried out using Lambda-950 spectrophotometer (PerkinElmer) as described in ref. 4. The integrated fluorescence (I) was calculated by integrating the intensity vs. time data obtained from fluorescence lifetime imaging microscopy measurements. n is the effective index of the medium in which the dye molecules are dispersed. The apparent quantum yield is calculated using Eq. **S7**.

$$\frac{(\Gamma_r)_{sample}}{(\Gamma_r)_{ref}} = \frac{\tau_{ref}}{\tau_{sample}} \cdot \frac{A_{ref}}{A_{sample}} \cdot \frac{I_{sample}}{I_{ref}} \cdot \left(\frac{n_{sample}}{n_{ref}}\right)^2, \quad \textbf{[S6]}$$

$$Q = \frac{\Gamma_r}{\Gamma_r + k_{nr}} = \Gamma_r \tau. \quad \textbf{[S7]}$$

1. Narayan J, et al. (1992) Epitaxial growth of TiN films on (100) silicon substrates by laser physical vapor deposition. *Appl Phys Lett* 61(11):1290–1292.
2. Fork DK, Ponce FA, Tramontana JC, Geballe TH (1991) Epitaxial MgO on Si(001) for Y-Ba-Cu-O thin-film growth by pulsed laser deposition. *Appl Phys Lett* 58(20): 2294–2296.
3. Novotny L, Hecht B (2006) *Principles of Nano-Optics* (Cambridge Univ Press, Cambridge, UK).
4. Kim J, et al. (2012) Improving the radiative decay rate for dye molecules with hyperbolic metamaterials. *Opt Express* 20(7):8100–8116.

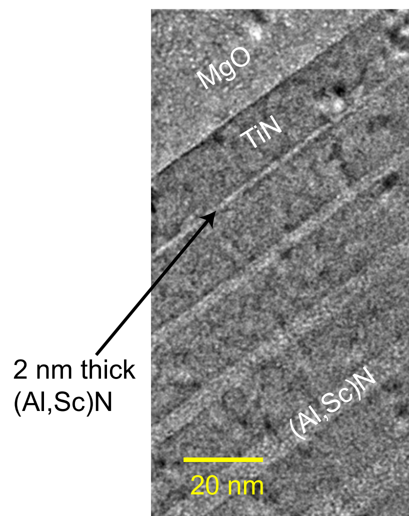

Fig. S1. Cross-sectional TEM image of a test sample consisting of a TiN–$Al_{0.72}Sc_{0.28}N$ superlattice with varying thickness of $Al_{0.72}Sc_{0.28}N$. The superlattice is grown on [001] MgO substrate and the thickness of TiN layer is maintained constant at 20 nm. The thinnest layer of (Al,Sc)N grown in the superlattice is 2 nm, as indicated in the figure.

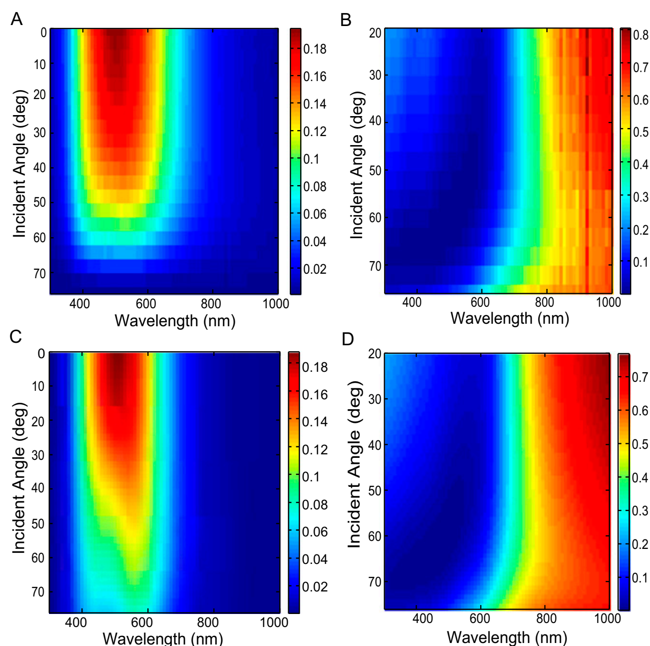

Fig. S2. Reflection and transmittance measurements. (*A* and *B*) Measured transmittance and reflectance, respectively, of a superlattice consisting of 16 pairs of 5-nm TiN and 5-nm (Al,Sc)N layers. (*C* and *D*) Calculated transmittance and reflectance, respectively. The calculations used the optical properties of TiN and (Al,Sc)N extracted from ellipsometry as shown in Fig. 2 *A* and *B*.

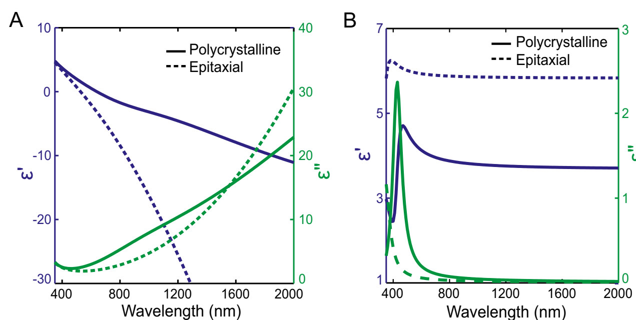

Fig. S3. Dielectric functions retrieved from spectroscopic ellipsometry measurements on epitaxial and polycrystalline TiN–AlScN superlattices: dielectric functions of 10-nm-thick layers of (*A*) TiN and (*B*) (Al,Sc)N.

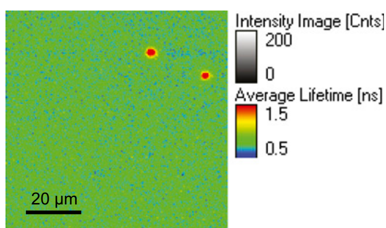

Fig. S4. Map of lifetime and fluorescence intensity from emitters placed on top of a sample. This map is a typical one showing the uniformity of the measured lifetimes. The red spots on the top right are believed to be arising from dust particles settling on the sample during spin-coating.